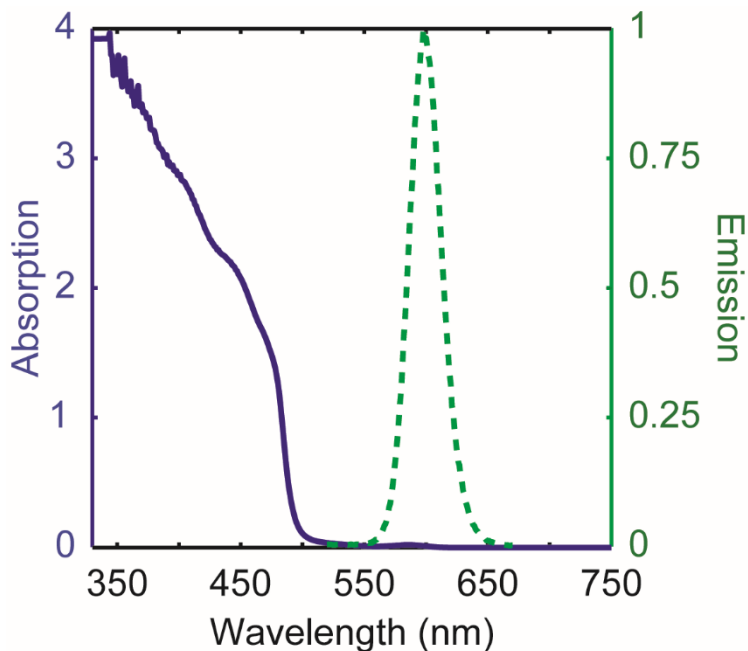


**Absorption and emission spectra of luminophore**



**Figure S1:** (solid) Absorption and (dashed) normalized emission spectra of CdSe/CdS dot-in-rod heterostructures. The nanocrystal properties are derived from Reference 1.

Figure S1 shows the assumed absorption and emission spectra of the nanocrystal luminophore. The shape is taken from these measurements, but the optical density is defined to be 0.8. In the figure, the emission is normalized for clarity. The characteristics of the Bragg mirror are shown in Figure S2.

## Reflectance of 1D Bragg mirror as a function of angle and wavelength

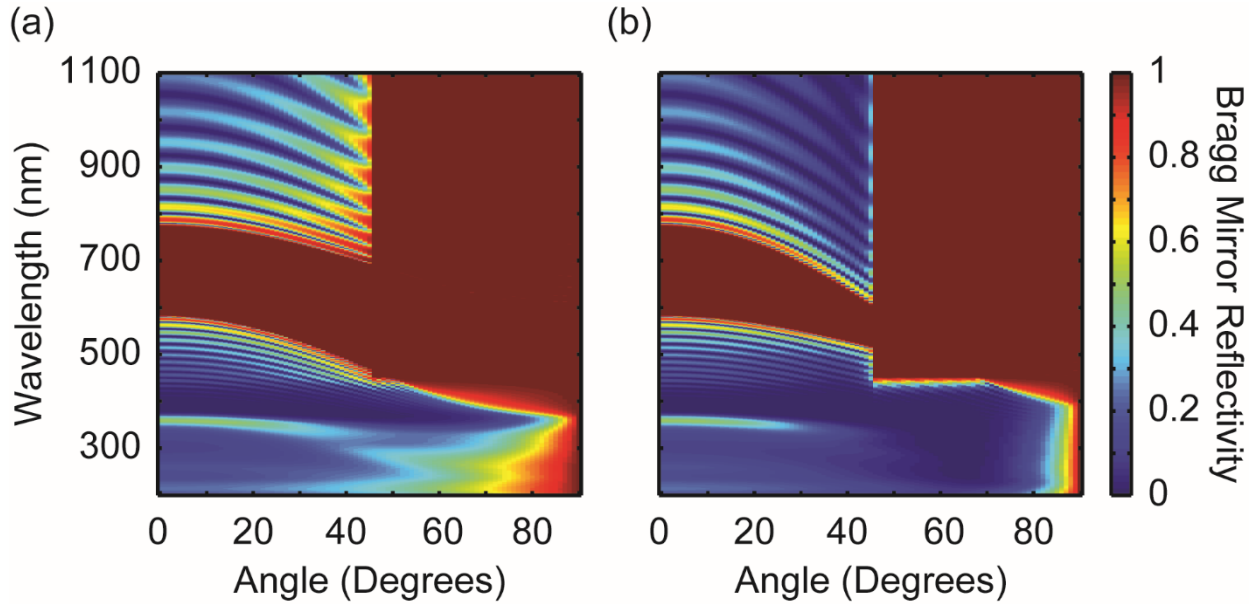


**Figure S2:** Probability of reflection from a 1D Bragg mirror for (a) s and (b) p polarized light.

The bandgap of the Bragg mirror is tuned to match the emission spectrum of the heterostructures from Figure S1. The properties of the Bragg mirror are derived from Reference 1.

### Simulation method: Monte Carlo ray-tracing model

**Overview of Ray-Tracing Algorithm:** A photon is injected with an angle perpendicular to the top face, at a position defined by the grid of possible injection locations inputted by the user, and with a wavelength in the range of interest for the simulation (330 – 700 nm). This photon is tracked through the LSC where it may be absorbed by the luminophores, reflected or refracted at the faces of the polymer waveguide, reflected or lost to the mirrors surrounding the LSC, reabsorbed by the luminophores, or collected by the solar cell.

When the photon is in the luminescent layer, defined as the 75  $\mu\text{m}$  layer in the center of the polymer waveguide, the photon can be absorbed. The probability that the photon is absorbed in the luminescent layer is given by

$$P_a = 1 - 10^{-\frac{OD Abs(\lambda)}{Abs(\lambda=450)t}}$$

where  $OD$  is the optical density of the luminescent layer defined at 450 nm,  $Abs(\lambda)$  is the absorption spectrum of the luminophore at the wavelength of the photon, and  $t$  is the distance travelled through the luminescent layer. If the photon is absorbed by the luminophore then it is assumed that a new photon will be emitted isotropically with a random polarization direction. The efficiency of this emission process is equal to the quantum yield of the luminophore. In the cases where the desired outcome is to couple all light into the TIR modes, then the photon is emitted with an angle greater than or equal to the desired angle and a random polarization direction. The wavelength of the emitted photon is drawn from the normalized emission spectrum of the luminophore.

If the photon is successfully emitted from the QD then it can interact with the faces of the polymer waveguide. The probability of reflection at these interfaces is determined by the Fresnel equations.

$$r_s = \frac{n_1 \cos \theta_i - n_2 \cos \theta_t}{n_1 \cos \theta_i + n_2 \cos \theta_t}$$

$$r_p = \frac{n_2 \cos \theta_i - n_1 \cos \theta_t}{n_1 \cos \theta_t + n_2 \cos \theta_i}$$

Where  $n_1$  and  $n_2$  are the refractive indices of the incident and transmitted layers and  $\theta_i$  and  $\theta_t$  are the incident and transmitted angles respectively.

The photon can also refract into the air gap and interact with the mirrors that surround the concentrator. If it interacts with one of the specular mirrors it has a probability of reflection based on the reflection coefficient of the mirror. When the specular mirror successfully reflects the

photon it has the same angle of reflection as the angle of incidence. If the photon interacts with the Bragg mirror then it has a probability of reflection based on its wavelength and angle of incidence. When the Bragg mirror successfully reflects the photon it has the same angle of reflection as the angle of incidence. If the photon interacts with the meta-mirror then it has a probability of reflection based on the reflection coefficient of the mirror. When the mirror successfully reflects the photon it has an angle based on the definitions in **Figure S3**.

When the photon is traveling within the luminescent layer it can also be reabsorbed by the luminescent layer due to the overlap between the absorption and emission spectra of the luminophore. The probability of absorption within the layer is calculated the same way as discussed previously changing  $\lambda$  to the new wavelength of the photon. Once the ray reaches the right side of the polymer waveguide it is collected by the solar cell. It is assumed that all photons that reach the solar cell face are collected.

This algorithm is performed for each wavelength of interest and each grid location on the top face of the polymer waveguide. The grid spacing is altered with the size of the concentrator such that 641,601 photons are injected on the top face for each wavelength of interest.

**Outputs:** The Monte Carlo Simulation determines the mechanism that each photon reached. Photons collected by the solar cell correspond to photons that have exited the right face of the polymer waveguide. Non-radiative loss contains photons that were lost to a non-radiative pathway after being absorbed once by a luminophore, as defined by the quantum yield. Reabsorbed non-radiative loss correspond to photons that have been successfully emitted from a luminophore at least once and then are reabsorbed and lost non-radiatively. These two categories are separated because the reabsorption losses are affected by the light propagation, whereas the non-radiative loss is defined solely by the quantum yield of the luminophore defined in the calculations. Escape

cone loss are photons which have been emitted from the luminophore and escape out of the top face of the polymer. Photons can also interact and be lost to a mirror or pass through the concentrator without being absorbed.

### **Design of meta-mirrors**

In simulations with a meta-mirror on the bottom the mirror follows the generalized form of Snell's law.

$$\theta_r = \sin^{-1}(\sin \theta_i + \delta)$$

Where  $\theta_i$  is the incident angle and  $\theta_r$  is the reflected angle. In the ideal case it is assumed that when  $\sin \theta_i + \delta > 1$  the incident photon is scattered into a surface wave propagating along the mirror dielectric interface. In the non-ideal case photons are reflected specularly or into higher order modes when the photon would be scattered into a surface mode.<sup>2</sup> In these simulations it is assumed that the photon is reflected specularly if it would be scattered into a surface mode.

The different phase shifting parameters in the main body of the paper were chosen to explore the difference between large and small angular shifts. A value of  $\delta = \frac{1}{n_{\text{polymer}}} \sim 0.67$  was chosen to reflect the photon into the region where it is reflected specularly after a few interactions with the meta-mirror. For normal incidence this mirror reflects the photon into a total internal reflection mode. After interacting with the meta-mirror the photon has an angle between 19 and 90 degrees before it is reflected specularly. A value of  $\delta = 1 - \frac{1}{n_{\text{polymer}}} \sim 0.33$  was chosen because this meta-mirror shifts the angle of the photon until it has an angle greater than the critical angle for the polymer/air interface, which is approximately 42°. Therefore, the photon has an angle between 42 and 90 degrees before it is reflected specularly. However, the meta-mirror imparts a smaller phase shift with each interaction with the incident photon. Therefore, the photon has to

interact with the meta-mirror more often before it reaches its final angle. The reflected angle for each incident angle is shown for both phase shifting parameters in **Figure S3**.

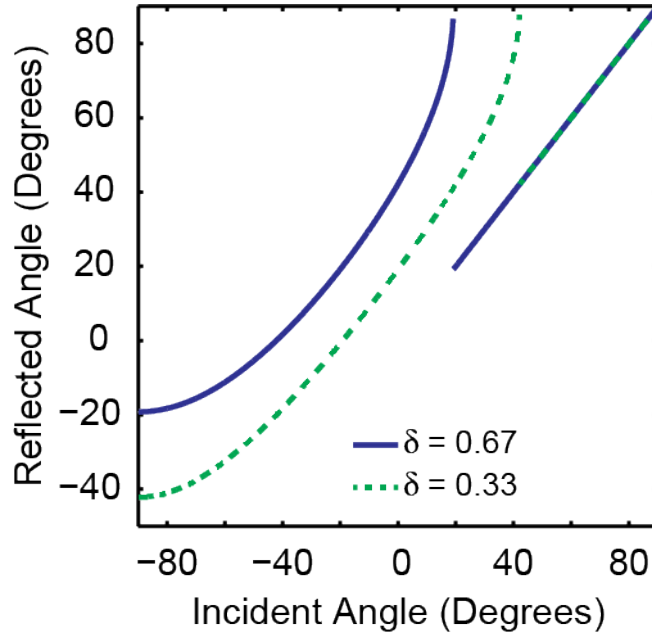


**Figure S3:** Reflected angle vs. incident angle using generalized Snell's law with the assumption that if the photon would be scattered into a surface mode it is instead reflected specularly. (solid)

Meta-mirror with a  $\delta$  of  $\frac{1}{n_{\text{polymer}}} \sim 0.67$ . (dashed) Meta-mirror with a  $\delta$  of  $1 - \frac{1}{n_{\text{polymer}}} \sim 0.33$ .

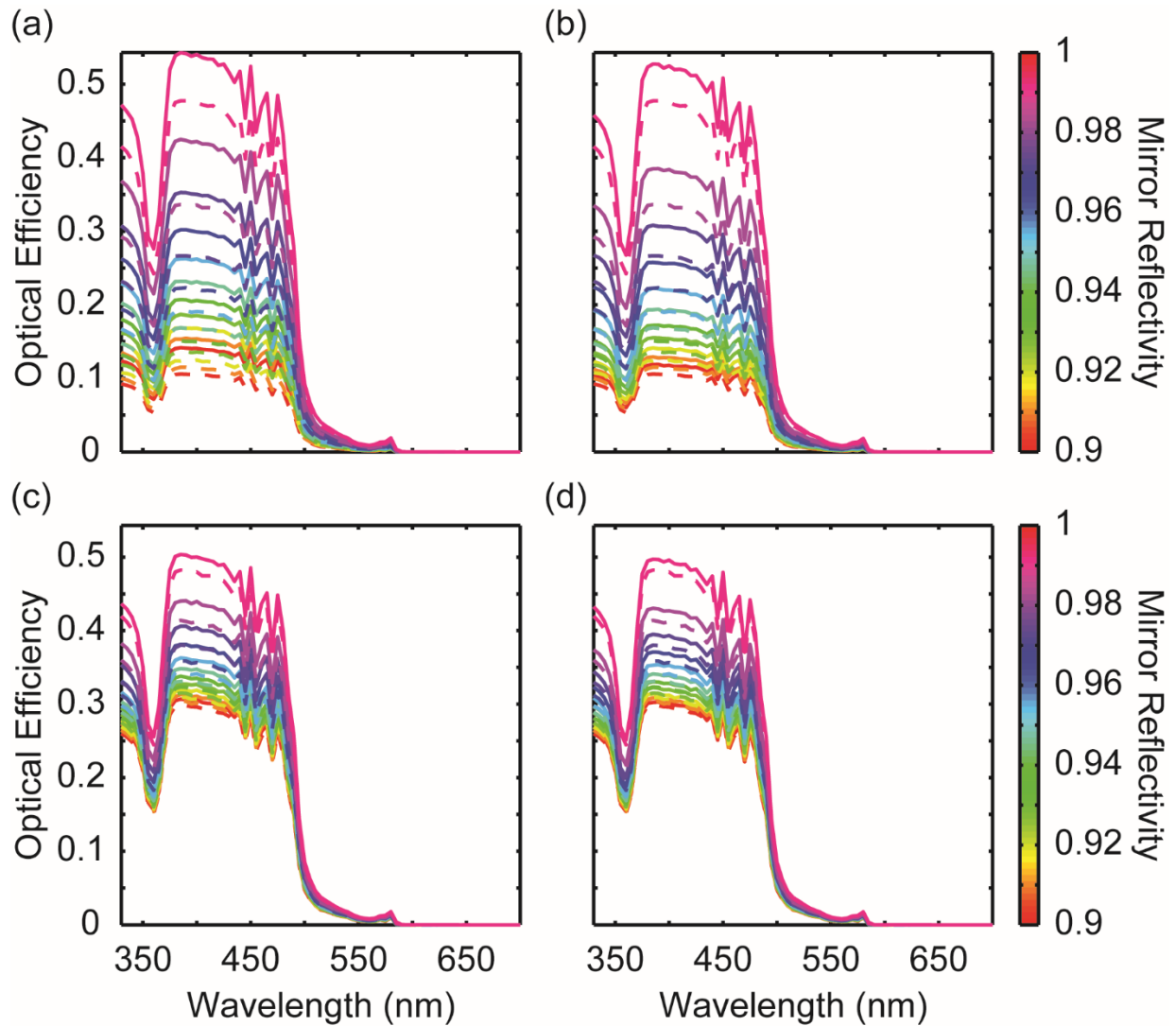


**Figure S4:** Comparison of optical efficiency between (solid) meta-mirror and (dashed) specular mirror for varying mirror reflectivity. (a) Meta-mirror with  $\delta$  of 0.33 and specular mirror without an air gap between the polymer waveguide and bottom mirror. (b) Meta-mirror with  $\delta$  of 0.67 and specular mirror without an air gap. (c) Meta-mirror with  $\delta$  of 0.33 and specular mirror with a 10  $\mu\text{m}$  air gap between the polymer waveguide and bottom mirror. (d) Meta-mirror with  $\delta$  of 0.67 and a 10  $\mu\text{m}$  air gap.

In **Fig. S4** the different meta- mirrors are compared to a specular bottom reflector, and are shown with full spectral resolution. The main text shows these results weighted by the solar spectrum according to

$$\eta_{SS} = \int_{330}^{500} \frac{\eta P_{\lambda}}{P_{330-500}} d\lambda$$

where  $\eta_{SS}$  is the solar spectrum weighted optical efficiency,  $\eta$  is the optical efficiency at a single wavelength,  $P_{\lambda}$  is the power in the binned solar spectrum for that wavelength, and  $P_{330-500}$  is the total power in the solar spectrum over the spectral range from 330 to 500 nm. Based on the spectral resolution of the calculations, the AM1.5G solar spectrum was divided into bins that represent the power in that range of wavelengths. Based on **Fig. S4**, the spectral characteristics track mainly with the Bragg mirror, with an increase in overall optical efficiency.

The results indicate that between these two cases, it is more favorable to use a smaller  $\delta = 0.33$  vs.  $\delta = 0.67$ . **Figure S5** elaborates on the role of  $\delta$  in the overall optical efficiency. Assuming that the meta-mirrors exhibit some loss due to the complex nanostructures, it is more favorable to include an air gap in the design as direct contact is only preferred when the reflectivity is extremely high. In that case and as mentioned in the main text, it is not possible to use the change in reflected angle to couple light into the TIR modes of the polymer, and coupling that changes the angle by small amounts is preferred. If the angular change is too small, however, the mirror simply becomes specular and there is no additional advantage to including the meta-mirror. This predicts that there should be an optimal value. To test this prediction, additional simulations were performed for a range of  $\delta$  as a function of mirror reflectivity, and weighted by the solar spectrum from 330 to 500 nm.

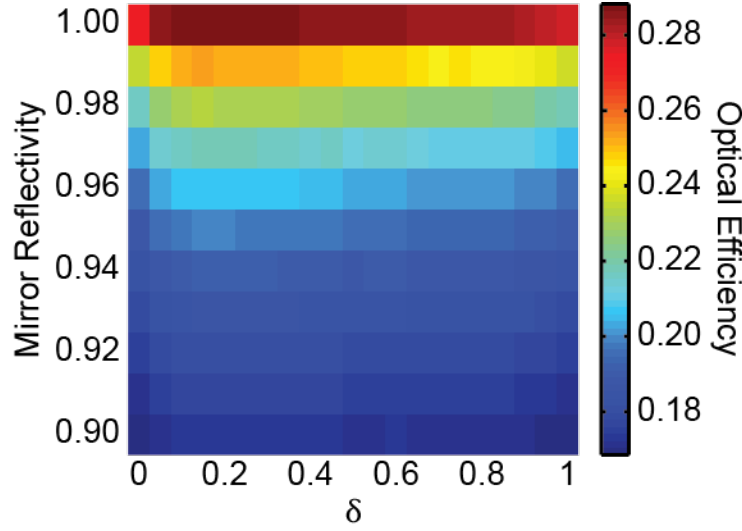


**Figure S5:** Comparison of solar spectrum weighted optical efficiency for different meta-mirrors. There is an air gap between the phase shifting mirror and the polymer waveguide.

From inspection of the data the optical efficiency is highest at low but non-zero values of  $\delta$ , reaching a maximum at approximately  $\delta = 0.2$ . The margins are in excess of the error estimates on the Monte Carlo calculations. Overall it is notable how little difference in performance is predicted by tuning the phase shift, which is promising for future fabrication.

From these calculations, we show an example of a gap plasmon-based metasurface that meets these requirements (Fig. S6). We follow the method described in Ref. 2. The period of the repeating structure ( $\Gamma$ ) is related to the gradient of the phase shift

$$\frac{d\phi(x)}{dx} = \frac{2\pi}{\Gamma} = \delta nk = \frac{\delta n 2\pi}{\lambda}$$

Therefore for the case where we assume an air gap ( $n = 1$ ), and are targeting 600 nm luminescent light and  $\delta = 0.2$ :

$$\Gamma = \frac{2\pi}{\delta kn} = \frac{2\pi\lambda}{\delta n 2\pi} = \frac{600 \text{ nm}}{0.2} = 3000 \text{ nm}$$

For simplicity we assume that the metal surface is dispersionless over the band of the luminescence and has a complex refractive index of  $n = -7i$ . We use finite difference time domain simulations to design the structure. For a 3000 nm period, we assume that 10 sub-cells of 300 nm are used, each containing a nanostructure of a particular width. The full set of 10 sub-cells are designed to span the entire  $2\pi$  phase shift, with each sub cell contributing  $2\frac{\pi}{10}$  phase shift. Simulations are performed on the individual sub-cells to extract the phase from a variety of different nanostructure widths, then the widths were chosen to achieve linear gradation in phase over the 3000 nm unit cell. The final chosen widths are tabulated below, based on the data shown in Fig. S7(a).

|      |       |       |       |         |       |       |       |       |       |
|------|-------|-------|-------|---------|-------|-------|-------|-------|-------|
| 0 nm | 56 nm | 60 nm | 61 nm | 62.5 nm | 63 nm | 64 nm | 65 nm | 68 nm | 80 nm |
|------|-------|-------|-------|---------|-------|-------|-------|-------|-------|

Simulations are then performed on this structure as a function of angle of incidence, as shown in Fig. S7(b), which shows the fraction of power at each angle of incidence coupled to each outgoing angle of reflection. This structure is not necessarily designed to be the optimal metasurface for this application, but is an example of a metasurface that fulfills the design criteria, and becomes more of a specular mirror as the angle of incidence becomes steeper.

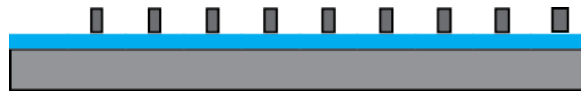


**Figure S6:** Schematic of a metasurface mirror, with the widths given in the table above. The dielectric layer has a thickness of 5 nm, and each metal block is 10 nm tall.

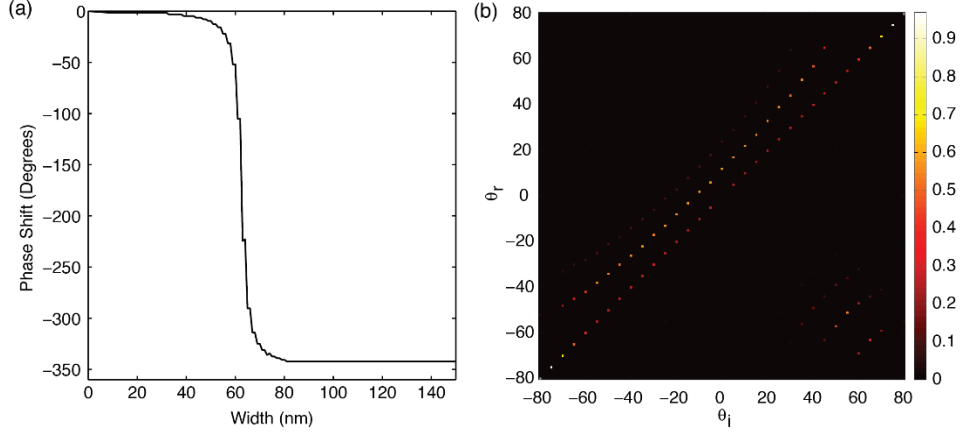


**Figure S7:** (a) Calculated phase shift at different widths of the top metal block, calculated in 300 nm unit subcells. (b) After a full array is designed consisting of 10 sub-cells, each containing a single nanoblock with the width in the table, the array is 3000 nm in length. This calculation shows the incident angle and reflected angle, with the fraction going into each angle represented by the color axis.

### Estimation of the impact of QD embedding on polymer refractive index

In the current work it is assumed that the polymer with nanocrystal luminophores has the same refractive index as the rest of the polymer waveguide. A calculation of the effective refractive index of the polymer/nanocrystal composite is presented to show that this assumption is reasonable. First the volume fraction is determined:

$$V_F = \frac{V_{QD}}{V_{LL}}$$

Where  $V_F$  is the volume fraction,  $V_{QD}$  is the volume of the quantum dots, and  $V_{LL}$  is the volume of the layer with QDs.

$$n_{moles_{QD}} = C V_{LL}$$

$$\#QD = n_{moles_{QD}} N_a$$

$$V_F = C N_a V_{QD}$$

Where  $C$  is the concentration of the QDs in the polymer with units of  $\frac{\text{moles}}{\text{L}}$  and  $N_a$  is Avogadro's number. From Beer's law the concentration can be calculated.

$$C = \frac{OD}{\epsilon t_{LL}}$$

Where OD is the optical density of the luminescent layer,  $\epsilon$  is the molar absorptivity of the quantum dots, and  $t_{LL}$  is the thickness of the luminescent layer. Therefore,

$$V_F = \frac{OD N_a V_{QD}}{\epsilon t_{LL}}$$

In this equation the molar absorptivity is the least known value. In literature it has been shown that spherical QDs with volumes of  $1910 \text{ nm}^3$  have molar absorptivity coefficients of approximately  $8 \times 10^5 \frac{\text{M}}{\text{cm}}$ .<sup>3</sup> The nanocrystals in these simulations have significantly larger volumes of  $6500 \text{ nm}^3$  and therefore most likely have larger molar absorptivity coefficients in the range of  $10^6 - 10^7 \frac{\text{M}}{\text{cm}}$ . Therefore, for an optical density of 0.8 and luminescent layer thickness of  $75 \mu\text{m}$ , the range of possible volume fractions is  $0.007 - 0.07$ . Using these volume fractions and the Maxwell-Garnett theory the refractive index of the luminescent layer can be estimated.<sup>4</sup>

$$\epsilon_{eff} = \epsilon_p \frac{2\delta_{QD}(\epsilon_{QD} - \epsilon_p) + \epsilon_{QD} + 2\epsilon_p}{2\epsilon_p + \epsilon_{QD} + \delta_{QD}(\epsilon_p - \epsilon_{QD})}$$

Where  $\epsilon_p = 2.22$  is the permittivity of the polymer,  $\epsilon_{QD}$  is the permittivity of the quantum dots, estimated to be  $5.81 + 2.67i$ ,<sup>5</sup> and  $\delta_{QD}$  is the volume fraction of the quantum dots. The range of real refractive indices found using the approximation is  $1.49 - 1.54$ . This calculation shows that

the assumption that the refractive index does not change is a reasonable one as the refractive index of the luminescent layer changes by less than 5% due to the addition of the quantum dots.

### References:

- (1) Bronstein, N. D.; Li, L.; Xu, L.; Yao, Y.; Ferry, V. E.; Alivisatos, A. P.; Nuzzo, R. G. Luminescent Solar Concentration with Semiconductor Nanorods and Transfer-Printed Micro-Silicon Solar Cells. *ACS Nano* **2014**, *8* (1), 44–53.
- (2) Khan, M. R.; Wang, X.; Bermel, P.; Alam, M. A. Enhanced Light Trapping in Solar Cells with a Meta-Mirror Following Generalized Snell's Law. *Opt. Express* **2014**, *22* (S3), A973.
- (3) Sun, J.; Goldys, E. M. Linear Absorption and Molar Extinction Coefficients in Direct Semiconductor Quantum Dots. *J. Phys. Chem. C* **2008**, *112* (25), 9261–9266.
- (4) Choy, T. *Effective Medium Theory*; Clarendon Press: Oxford, 1999.
- (5) Ward, L. Cadmium Sulphide (CdS) A2 - Palik, Edward D. In *Handbook of Optical Constants of Solids*; Academic Press: Burlington, 1997; pp 579–595.